

Inhibition of neddylation induces mitotic defects and alters MKLP1 accumulation at the midbody during cytokinesis

Dudley Chung^a, Jayme Salsman^a, and Graham Dellaire ^{a,b,c}

^aDepartment of Pathology, Dalhousie University, Halifax, Canada; ^bDepartment of Biochemistry & Molecular Biology, Dalhousie University, Halifax, Canada; ^cBeatrice Hunter Cancer Research Institute, Halifax, Canada

ABSTRACT

The cullin-RING E3 ubiquitin ligases (CRLs) play crucial roles in modulating the stability of proteins in the cell and are, in turn, regulated by post-translational modification by the ubiquitin-like (Ubl) protein NEDD8. This process, termed neddylation, is reversible through the action of the COP9 signalosome (CSN); a multi-subunit metalloprotease conserved among eukaryotes that plays direct or indirect roles in DNA repair, cell signaling and cell cycle regulation in part through modulating the activity of the CRLs. Previously, inhibition of CRL neddylation by MLN4924, a small molecule inhibitor of the NEDD8-activating enzyme 1 (NAE1), was shown to induce interphase cell cycle arrest and cell death. Using fixed and living cell microscopy, we re-evaluated the cell cycle effects of inhibition of neddylation by MLN4924 in both asynchronous and mitotic cell populations. Consistent with previous studies, treatment of asynchronous cells with MLN4924 increased CDT1 expression levels, induced G2 arrest and increased nuclear size. However, in synchronized cells treated in mitosis, mitotic defects were observed including lagging chromosomes and binucleated daughter cells. Consistent with neddylation and deneddylation playing a role in cytokinesis, NEDD8, as well as subunits of the CSN, could be localized at the midbody and cleavage furrow. Finally, treatment of mitotic cells with MLN4924 induced the premature accumulation of MKLP1 at the cleavage furrow, a key regulator of cytokinesis, which was concomitant with increased abscission delay and failure. Thus, these studies uncover an uncharacterized mitotic effect of MLN4924 on MKLP1 accumulation at the midbody and support a role for neddylation during cytokinesis.

Abbreviations: CSN, COP9 Signalosome; MKLP1, mitotic kinesin-like protein 1; NEDD8, Neural precursor cell Expressed, Developmentally Down-regulated 8.

ARTICLE HISTORY

Received 16 June 2018
Revised 31 March 2019
Accepted 12 April 2019

KEYWORDS

COP9 signalosome;
MLN4924; NEDD8;
cytokinesis; midbody; MKLP1

Introduction

Somatic cell division in eukaryotic cells is tightly regulated to ensure fidelity in the transfer of genetic material between daughter cells. The final step in cell division is cytokinesis, and during cytokinesis in animal cells, an actomyosin contractile ring forms between daughter cells after the onset of anaphase and chromosome separation creating a structure known as the cleavage furrow [1]. The cleavage furrow constricts toward the center of the cell, drawing the plasma membrane with it, and eventually, only a narrow bridge of cytoplasm and a compact structure known as the midbody remain. The midbody plays a critical role in the final step of cytokinesis known as abscission; the process by which the intracellular bridge between the two daughter cells is severed. Altogether over 100 proteins have been found to

play a role in cytokinesis, including the mitotic kinesin-like protein 1 (MKLP1), also known as kinesin family member 23 (KIF23) [2,3]. MKLP1 belongs to the group of proteins known as chromosomal passengers; proteins that localize initially to chromosomes and centromeres but later re-locate to the spindle midzone and then the midbody, and includes the inner centromere protein (INCENP) and Aurora B kinase (AURKB) [4]. Recruitment of MKLP1 by INCENP to the midbody and its phosphorylation by AURKB is essential for completion of cytokinesis [5,6]. As such, loss of these passenger proteins results in cytokinesis defects including delayed or failed abscission [4]. In turn, failure of cytokinesis can result in cell death or, if the cell survives, genomic instability by promoting aneuploidy that in turn can drive cancer development and progression [7].

CONTACT Graham Dellaire  dellaire@dal.ca

 Supplemental data for this article can be accessed [here](#).

© 2019 The Author(s). Published by Informa UK Limited, trading as Taylor & Francis Group.
This is an Open Access article distributed under the terms of the Creative Commons Attribution-NonCommercial-NoDerivatives License (<http://creativecommons.org/licenses/by-nc-nd/4.0/>), which permits non-commercial re-use, distribution, and reproduction in any medium, provided the original work is properly cited, and is not altered, transformed, or built upon in any way.

During cell division, mitotic kinases like AURKB phosphorylate a number of substrate proteins, leading to spatial-temporal changes in their localization and/or function [8]. However, several other protein modifications also play important roles in cell division including modification by ubiquitin and members of the ubiquitin-like protein (Ubl) family [9], such as the small ubiquitin-related modifier (SUMO) [10] and neural precursor cell expressed, developmentally down-regulated 8 (NEDD8) [11]. The covalent attachment of ubiquitin (or the UbIs) occurs at receptor lysine residues located on target proteins and is mediated by three classes of enzymes, termed E1, E2 and E3 (see [12] for a comprehensive discussion). During cell division, ubiquitin-mediated proteolysis is primarily done by the anaphase-promoting complex/cyclosome (APC/C) and cullin-RING ubiquitin ligases (CRLs). For example, the degradation of cyclin B1 by APC/C and CRL2-ZYG11 is required for progression through mitosis in *C. elegans* and human cells [13]. In another example, targeted degradation of chromatin licensing and DNA replication factor 1 (CDT1) and Geminin in G2 and G1 (respectively) prevents re-replication of DNA during the cell cycle [14]. Degradation of CDT1 in G2 occurs via the action of either the Skp, cullin, F-box (SCF) complex (SCF-Skp2) or the DDB1-CUL4 E3 ligase complex [15,16], and Geminin is degraded by APC-CDH1 at the metaphase-anaphase transition and during G1 [17].

The activity of the CRLs, including CUL1, 2, 3, 4A/B, and CUL5, is regulated by modification with the Ubl NEDD8 [9]. Covalent attachment of NEDD8, referred to as neddylation, occurs via the action of a single E1, NAE – a heterodimer of NEDD8-activating enzyme NAE1 and UBA3, and the E2 enzymes UBE2M (UBC12) and its orthologue UBE2F [12]. NEDD8 is thought to activate CRLs by promoting the reconfiguration of the complex to its active state [18], which allows the ubiquitin E2, carrying the charged ubiquitin, to interact with the cullin complex. Thus, the activity of the CRLs can be tightly regulated by NAE-dependent neddylation, and consequently reversibly inhibited by deneddylation [19].

Deneddylation of the CRLs occurs primarily via the action of the evolutionarily conserved COP9 signalosome (CSN) [20–22]; however, when NEDD8 is overexpressed, hyper-neddylated CRLs can be deneddylated by SENP8 (also known as

DEN1) [23,24]. The COP9 signalosome (CSN) consists of eight subunits (CSN1 to CSN8, also known as COPS1-8) [19,22], and each subunit contains C-terminal α -helices that allow it to associate with the other subunits [25]. Of the CSN subunits, CSN5 encodes the enzymatic activity of the complex. Structurally, CSN5 and CSN6 contain an MPN (MPR-PAD1-Nterm) domain and the other subunits contain a PCI (Proteasome, COP9 signalosome, Initiation factor 3 eIF-3) domain, which are believed to mediate protein–protein interactions [25]. Of note, CSN5 and CSN6 are known to form a stable subcomplex with subunits CSN4 and CSN7A/B, and CSN6 is important in the incorporation of CSN5 in the catalytically active CSN complex [18,25,26].

The CSN has been implicated in development, cell differentiation, DNA repair and cell cycle control in response to various cell stresses across multiple phyla [20,21,27,28]. Many insights into the biological function(s) of neddylation have been revealed by inhibition of NAE1 by the small molecule MLN4924, which indirectly inhibits a broad range of CRLs by blocking their neddylation [29]. Inhibition of neddylation by MLN4924 has been shown to have anti-cancer activity *in vitro* and *in vivo*, and results in the accumulation CDT1, re-replication of DNA in S-phase and G2 arrest [29–32].

Using fixed and live-cell microscopy, we re-evaluated the cell cycle effects of inhibition of neddylation by MLN4924 in both asynchronous and mitotic cell populations. As expected, MLN4924 treatment of asynchronous cells resulted in the accumulation of CDT1, G2 arrest and increased nuclear size consistent with re-replication of DNA. However, in synchronized cells treated in mitosis, we observed mitotic defects including lagging chromosomes and binucleated daughter cells. Consistent with neddylation playing a role in cytokinesis, we also localized NEDD8 and CSN subunits to the midbody and cleavage furrow. Finally, treatment of synchronized cells prior to mitosis with MLN4924, induced premature accumulation of MKLP1 to the cleavage furrow and increased abscission failure. Thus, these studies uncover a previously uncharacterized cell cycle effect of MLN4924 on MKLP1 accumulation at the midbody and support a role for neddylation during cytokinesis.

Results

Inhibition of neddylation by MLN4924 leads to CDT1 accumulation, G2 arrest and the increased numbers of cells with more than 4N DNA content

To establish drug potency and re-examine the cell cycle effects of neddylation inhibition we treated asynchronous HeLa cells with 0.3 μ M MLN4924 for 24 to 48 h and used the ES-FUCCI (Fluorescent, Ubiquitination-based Cell Cycle Indicator [33]) reporter system [34] to monitor the levels of the CRL substrate CDT1 degraded in G1/S (mCherry-CDT1), and the APC-CDH1 substrate Geminin (Citrine-Geminin) degraded in G2/M (Figure 1). We observed a significant increase in CDT1 expression in MLN4924-treated cells over time as measured by the integrated fluorescent intensity of mCherry-CDT1 per cell ($p < 0.0001$), a result consistent with previous findings that MLN4924 treatment above 0.25 μ M can strongly block neddylation and stabilize CDT1 [29,35]. MLN4924 treatment for 48 h also increased Citrine-Geminin expression, which is not a CRL substrate, indicating that cells not initially arrested in G1/S began to accumulate in G2. These effects on CDT1 and Geminin in MLN4924-treated cells correlated with reduced protein neddylation, including CUL1 modification by NEDD8, as measured by Western blot (Supplementary Figure S1). We also analyzed the cell cycle distribution of vehicle (DMSO) and MLN4924-treated cells by flow cytometry (Figure 2 (a–b)). We observed a trend between 24 and 48 h of decreasing numbers of cells in G1 ($p < 0.01$ at 48 h) and increasing numbers of cells in G2/M with 4N DNA content ($p < 0.05$ at 48 h), in addition to the accumulation of cells with >4N DNA content between drug-treated and vehicle (DMSO)-treated cells ($p < 0.01$ at 48 h). Similarly, we found that treatment of the Tert-immortalized normal human fibroblast cell line GM05757 [36] with MLN4924 resulted in the appearance of cells with giant nuclei consistent with endoreplication of DNA (Supplementary Figure S2). Finally, we also observed G2 arrest in MLN4924-treated cells that coincided with a significant increase in nuclear area overtime (Figure 2(c), $p < 0.0001$). These results are consistent with previously reported G2 cell cycle arrest and the endoreplication of DNA in S-phase cells due to the accumulation of CDT1 in cells treated with MLN4924 [29].

NEDD8 and the COP9 signalosome localize to the midbody with cullins 1 and 3 during cytokinesis

The presence of >4N cells after 48 h of MLN4924 treatment (Figure 2) could arise by either DNA endoreplication or by errors in cell division during mitosis that could contribute to aneuploidy [37]. Given that CRL E3 ubiquitin ligases are implicated in mitotic progression [38–41], this prompted us to ask whether neddylation is also involved in cytokinesis. To test this hypothesis, we examined the localization of NEDD8, selected CRLs and subunits of the COP9 signalosome (CSN) by immunofluorescence microscopy of endogenous proteins and those tagged with fluorescent proteins in untreated HeLa cells (Figures 3 and 4). Endogenous NEDD8 was detected on either side of the cleavage furrow (Figure 3(a)) during early cytokinesis, and then more centrally at the midbody (Figure 3(b and c)), suggesting differential localization of neddylated proteins between early and late cytokinesis. The midbody localization of NEDD8 closely aligned with enhanced green fluorescent protein (EGFP)-CUL1 and endogenous CUL3, which are known neddylation substrates. We also observed CUL3 localization to the cleavage furrow in normal retinal pigment epithelial cell line RPE-1 (Supplementary Figure S3). These data are consistent with previous reports of CUL1 and CUL3 being identified as components of the midbody [38,40].

Using an antibody directed against CSN4, we localized this CSN subunit to the intercellular bridge and the outer edges of the midbody (Figure 3(c)). This prompted a more thorough examination of the localization of the other CSN subunits, which together form the CSN holoenzyme [18]. This was accomplished by using fluorescent protein fusions of the CSN subunits, which was necessary due to the paucity of antibodies available for this complex. Using DIC (differential interference contrast) and the MKLP1 protein to identify midbodies [5,6,42] within fluorescence micrographs, we found that all subunits could be localized to the midbody of untreated HeLa and RPE-1 cells, implying that the entire CSN complex is present there during cytokinesis (Figure 4, Supplementary Figure S3 and S4). In agreement with CRL and NEDD8 localization at the midbody, most CSN subunits fused to EGFP, or the red fluorescent

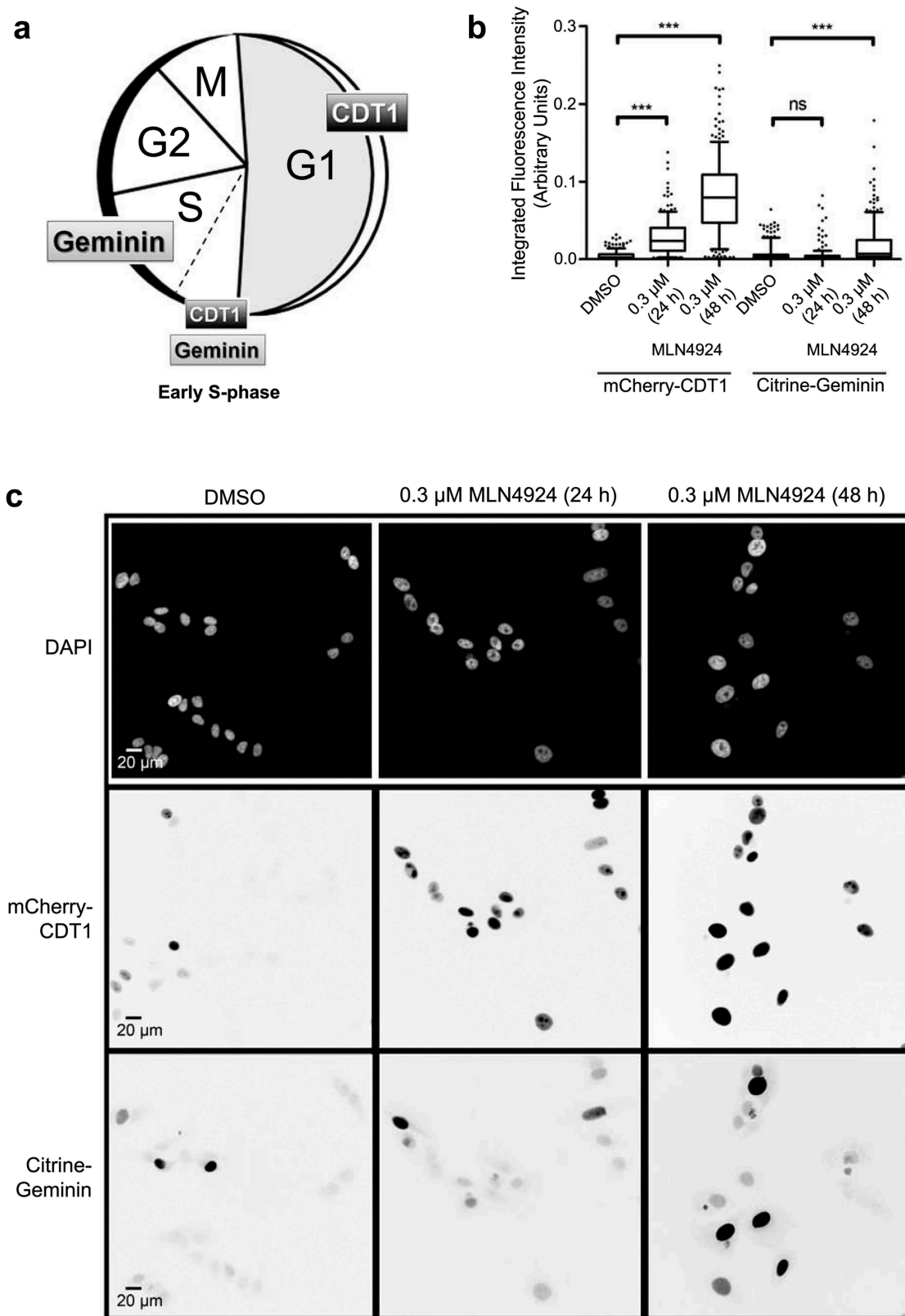


Figure 1. Elevated expression of mCherry-CDT1 and Citrine-geminin upon chemical inhibition of neddylation in asynchronous HeLa cells. (a) Overview of the FUCCI system, where CDT1 is expressed predominately in G1 and Geminin is expressed during S, G2 and Mitosis (M) phase of the cell cycle. Asynchronous HeLa cells stably expressing ES-FUCCI reporter were treated with vehicle (0.03% DMSO; N = 181 cells) or 0.3 μM MLN4924 for 24 h (N = 164 cells) and 48 h (N = 191 cells). (b) Integrated fluorescent intensity per cell is shown for mCherry-CDT1 (G1/S) and Citrine-Geminin (G2/M). Graphs are depicted as a box and whisker plot, where the mean, 9th and 91st percentile are depicted as horizontal bars, and the outliers beyond one standard deviation are plotted as individual points. Data were collated from three replicates, and the number of cells (N) evaluated for each condition is indicated. (c) Micrographs of mCherry-CDT1 and nuclei stained with DAPI are shown for cells treated with vehicle or 0.3 μM MLN4924 for 48 h and asterisks indicate the degree of significance between means (***) = $p < 0.0001$, ns = no significance).

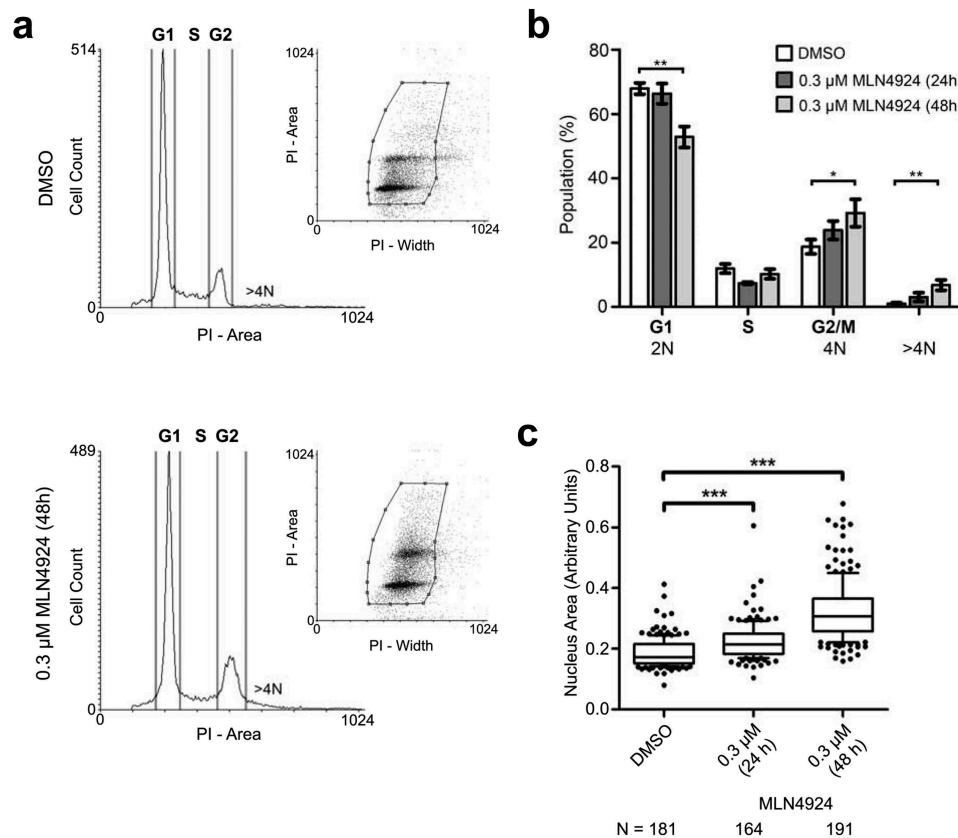


Figure 2. Cell cycle effects of chemical inhibition of neddylation on asynchronous HeLa cells. Asynchronous HeLa cells were treated with vehicle (0.03% DMSO) or 0.3 μM MLN4924 and collected 24 h and 48 h later for flow cytometry. (a–b) Representative histogram and dot plot of gated regions in untreated and treated populations (Panel A). Vertical lines delineate populations according to cell cycle phase (Panel B) Each bar is the mean percentage of cells in different cell cycle phases for four biological replicates. (c) Relative nuclear area (DNA stained with DAPI) was depicted as a box and whisker plot, where the mean, 9th and 91st percentile are depicted as horizontal bars, and the outliers beyond one standard deviation are plotted as individual points. Data were collated from three replicates, and the number of cells (N) evaluated for each condition is indicated. *** = $p < 0.0001$, ** = $p < 0.01$, * = $p < 0.05$.

protein mRuby2, tended to be localized toward the outer edge of the midbody forming a ring-like structure (e.g. CSN4 and CSN6) or were found in both the centre and the edge of the midbody (e.g. CSN5) (Figure 4(a)); a result that is in contrast with the faint localization of EGFP at the centre of the midbody, which is consistent with non-specific trapping of EGFP when not fused to a CSN subunit. Co-expression of pairs of CSN subunits also resulted in co-localization at midbodies in a ring pattern that overlapped with the immunofluorescence signal of endogenous MKLP1 (Figure 4(b)). We also observed the redistribution of CSN5 from more diffuse localization throughout the midbody when co-expressed

with CSN4 to a very distinct ring localization pattern with a central cavity when co-expressed with CSN6, indicating specific recruitment of CSN5 to the contractile ring by CSN6 (Figure 5(b)). Although signal intensity at the midbody imaged in the x/y dimension (with respect to the growth substrate) varied among the fluorescent protein-tagged CSN subunits, the mean fluorescence of several of the subunits exhibits significantly higher fluorescent intensities than EGFP alone, including CSN4 ($p < 0.01$), CSN6 ($p < 0.01$), CSN7A ($p < 0.001$), CSN7B ($p < 0.01$) and CSN8 ($p < 0.001$) (Figure 4(c)). In addition, we found that EGFP-CSN5 exhibited significantly lower fluorescent intensity at the midbody than EGFP alone ($p < 0.001$;

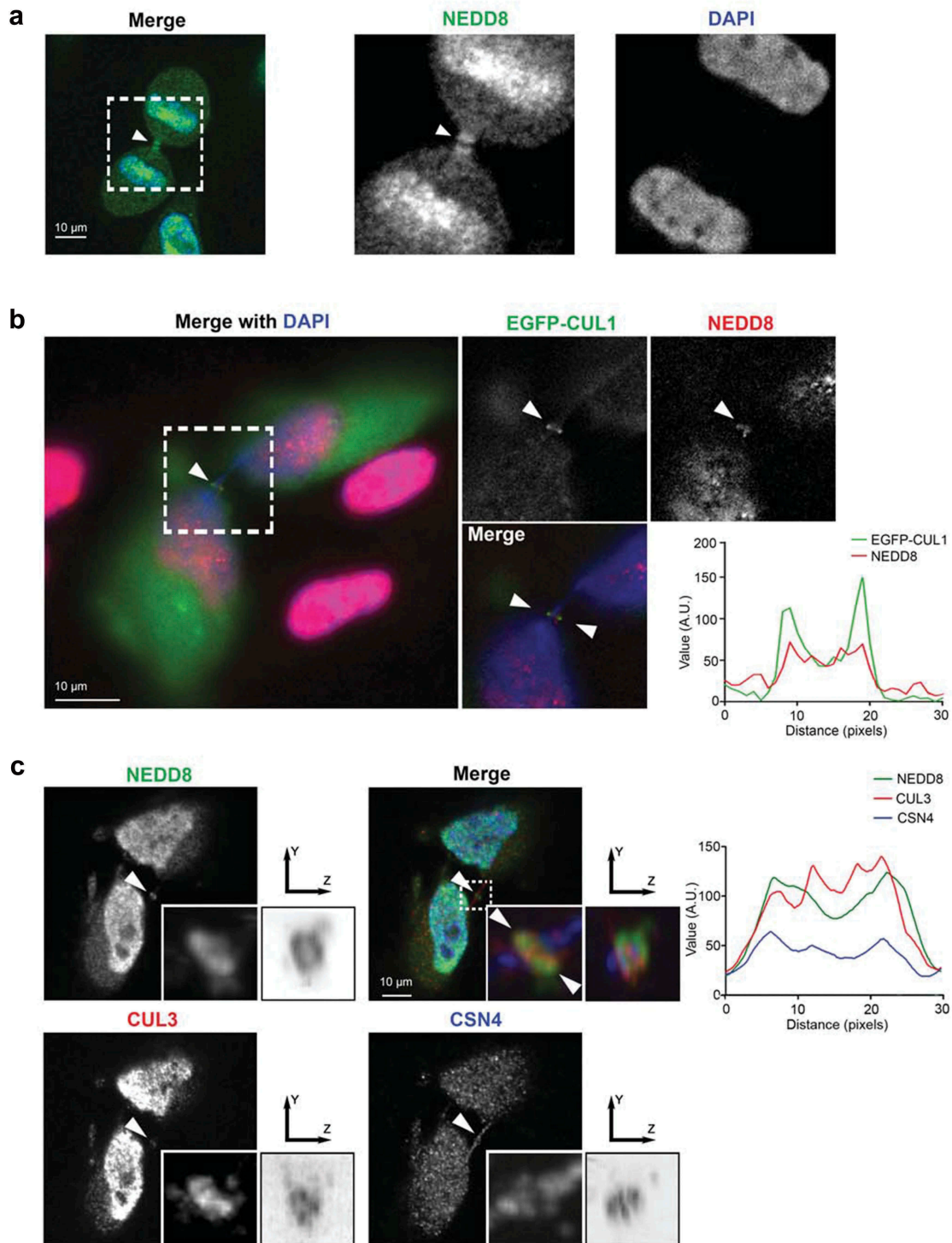


Figure 3. NEDD8 localizes at the cleavage furrow and midbody adjacent to Cullins 1 and 3. (a) Immunofluorescence detection of NEDD8 (green) at the cleavage furrow in untreated HeLa cells during early stages of cytokinesis. Magnified regions are indicated with white boxes, and the midbody is indicated (white arrowhead). DNA was stained with DAPI. (b–c) Co-immunofluorescence detection of NEDD8 (red) EGFP-CUL1 (green) (Panel B), and NEDD8 (green) with CUL3 (red), and CSN4 (blue) (Panel C) in HeLa cells. In Panel C magnified regions containing the midbody are shown for both *x/y* and *y/z* orientation. Line scan plots of the signal intensity across the midbody (bounded by opposite-facing arrowheads) are shown for each fluorescent channel.

Figure 4(c)), which we speculate may be because of tighter control of CSN5 protein levels compared to other CSN subunits.

Given the localization pattern and significantly higher fluorescence signal intensities of several of the fluorescent protein-tagged CSN subunits, we

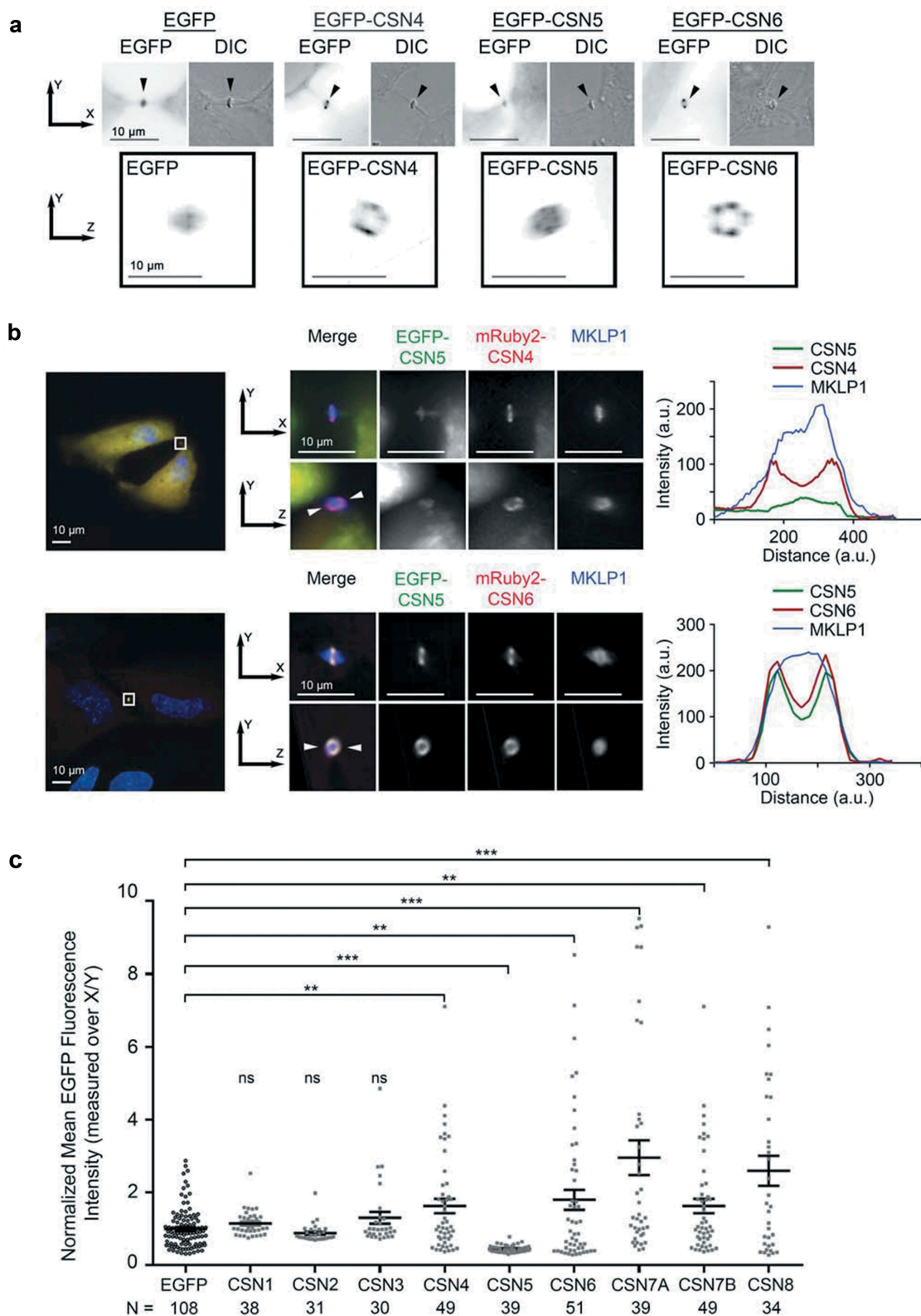


Figure 4. CSN subunits localize in distinct structures at the midbody during cytokinesis. (a) Representative images of EGFP-tagged CSN4, CSN5 and CSN6 expression at the midbody, which are identified using differential interference contrast (DIC) (black arrows). Boxed areas represent magnified images in the y/z orientation of the midbody for each fluorescence micrograph shown above in the x/y orientation. (b) Representative midbodies found in the image at the far left (white box) are shown at the right magnified to highlight the expression pattern of CSN subunits in both the x/y and y/z orientation. Double co-localization using transiently expressed EGFP-CSN5 (green), paired with mRuby2-CSN4 or CSN6 (red) at midbodies, as identified with MKLP1 antibody staining (blue). Line scan plots of the signal intensity across the midbody (bounded by opposite-facing arrowheads) are shown for each fluorescent channel. (c) Mean EGFP fluorescent signal intensity of all CSN subunits at midbodies was scored and compared with EGFP alone, with the data represented as vertical scatter plots with mean, SEM. The number of measurements made from individual cells (N), collated from three replicates, are shown below each scatter plot. Significance was determined using an unpaired Student's t-test with Welch's correction. ns = not significant, *** = $p < 0.001$, and ** = $p < 0.01$.

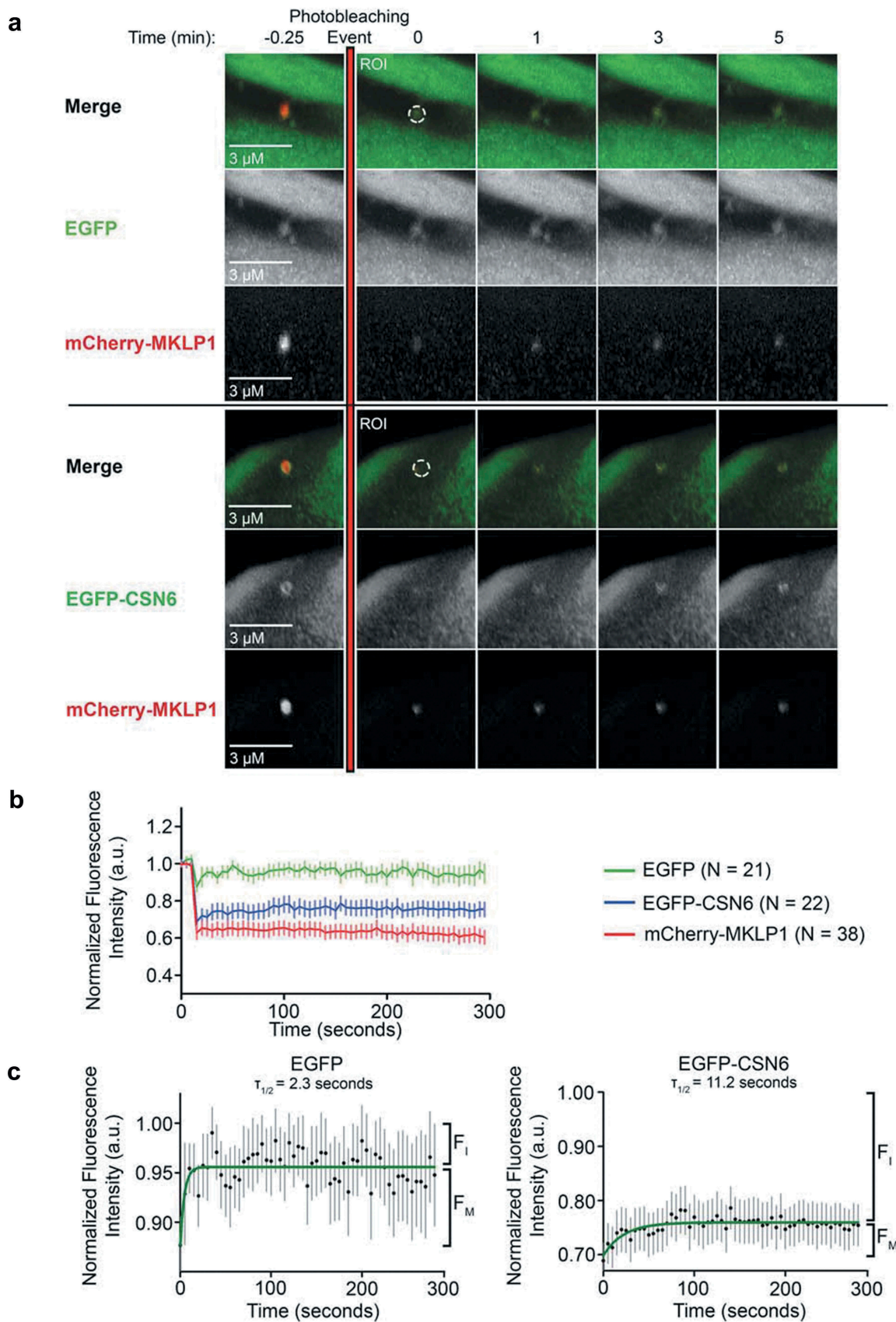


Figure 5. Measurement of EGFP versus EGFP-CSN6 fluorescence recovery after photobleaching (FRAP) at the midbody. (a) Representative images of EGFP, EGFP-CSN6 and midbody protein mCherry-MKLP1 before and after photobleaching. (b) The mean normalized fluorescence intensity is shown in the recovery curve for EGFP (green line), EGFP-CSN6 (blue line), and mCherry-MKLP1 (red line). The vertical bars show standard error of the mean. Data were collected for up to 5-min post-bleaching event. (c) A fitted curve (green line) of the data in Panel B was used to determine the mobile and immobile fraction (indicated as F_M and F_I , respectively) and the recovery half-life ($\tau_{1/2}$) for EGFP (left) and EGFP-CSN6 (right).

hypothesized that the COP9 signalosome was likely associated with the actin-contractile ring at the midbody, and as such would exhibit restricted diffusion in comparison to a freely diffusing fluorescent protein such as EGFP alone. Therefore, to further characterize the association of the CSN with the midbody, we examined the localization and diffusion of EGFP-CSN6 as a marker of the COP9 signalosome in HeLa cells by fluorescence recovery after photobleaching (FRAP) (Figure 5). In our bleaching experiments, we used the localization of mCherry-tagged MKLP1 as a fiduciary for the position of the midbody and employed a high intensity 488 nm laser to simultaneously bleach mCherry-MKLP1 and EGFP-CSN6 (or EGFP) at the midbody. Fluorescence recovery of EGFP was very rapid, while EGFP-CSN6 and mCherry-MKLP1 only recovered partially over the 5-min time period observed. By plotting the mean intensity of the fluorescent signal for EGFP and EGFP-CSN6, and curve fitted using a non-linear regression and the exponential one-phase association model, it was found that CSN6 has a larger immobile fraction than EGFP (Figure 5(b)); a result consistent with a strong association with substructures within the midbody such as the contractile ring.

MLN4924 treatment causes aberrant mitosis and the early accumulation of MKLP1 at the midbody concomitant with increased abscission failure

Treatment of asynchronous HeLa cells with the neddylation inhibitor MLN4924 produced a small subset of cells with greater than 4N DNA content (Figure 2). Given our data demonstrating neddylation substrates such as the cullins (i.e. CUL 1 and 3; Figure 3) and the CSN deneddylase complex at the midbody during cytokinesis, we sought to determine if we could find evidence of aberrant mitosis that might partly explain changes in DNA content per cell. We found upon further inspection that cells treated with the neddylation inhibitor MLN4924 for 48 h did indeed result in a significant increase in abnormal mitotic events compared to the control (Figure 6 and Supplemental Figure S5). These abnormal mitotic events included lagging chromosomes, chromosome bridges, asymmetric cell division, binucleated and multinucleated cells. Of note, NEDD8 could still be found to localize at the midbody in treated cells, which could indicate

the existence of either long-lived neddylation substrates or unconjugated NEDD8 at this structure (Supplemental Figure S5). These mitotic events could be related to the accumulation of cullin substrates during the extended treatment of cells with MLN4924. Thus, to gain additional insight into the role of neddylation specifically in mitosis, we treated HeLa cells collected by mitotic shake-off with MLN4924 and followed the progress of these mitotic cells as they entered cytokinesis by live-cell spinning-disk confocal microscopy (Figure 7, Supplemental Movies S1 (T = 0 @ 11 min) and S2 (T = 0 @ 16 min)). To facilitate live-cell imaging, HeLa cells transiently expressed GFP-MKLP1 to mark the midbody, mScarlet-i-LifeAct to label the actin cytoskeleton, and DNA was stained with the viable far-red dye SiR-DNA (Figure 7(a)). We observed that MKLP1 accumulated at the cleavage furrow and midbody in MLN4924-treated cells significantly earlier after the onset anaphase (18.3 ± 1.4 min, 95% CI: 15.4 to 21.2 min) than vehicle-treated cells (26.7 ± 3.5 min, 95% CI: 19.3 to 34.1 min) ($p < 0.01$; Figure 7(b)). Furthermore, when the cells were followed over a time course of 8 h, we observed a significant number of cells with delayed or failed abscission in the MLN4924 treated cells as compared to those treated with vehicle ($p < 0.0001$; Figure 8(a–b)). In addition, MKLP1 localization at the midbody became fragmented between 90 min and 180 min after the onset of anaphase in a subset of MLN4924-treated cells as they entered late telophase, which was concomitant with abscission delay (Figure 8(c), Supplemental Movie S2). Thus, ongoing neddylation in mitosis plays a role in regulating the accumulation of MKLP1 at the midbody and is required for efficient and timely abscission during cytokinesis.

Discussion

Protein neddylation in animal cells has been implicated in diverse cellular functions including epithelial-to-mesenchymal transition [43], autophagy [44], senescence [30,45], the DNA damage response [46,47], and cell cycle regulation [29,48]. Consistent with previous reports [29–32], we found that inhibition of neddylation by treatment of human HeLa cervical cancer and GM05757 fibroblast cells with the small molecule MLN4924 resulted in the accumulation of cells with

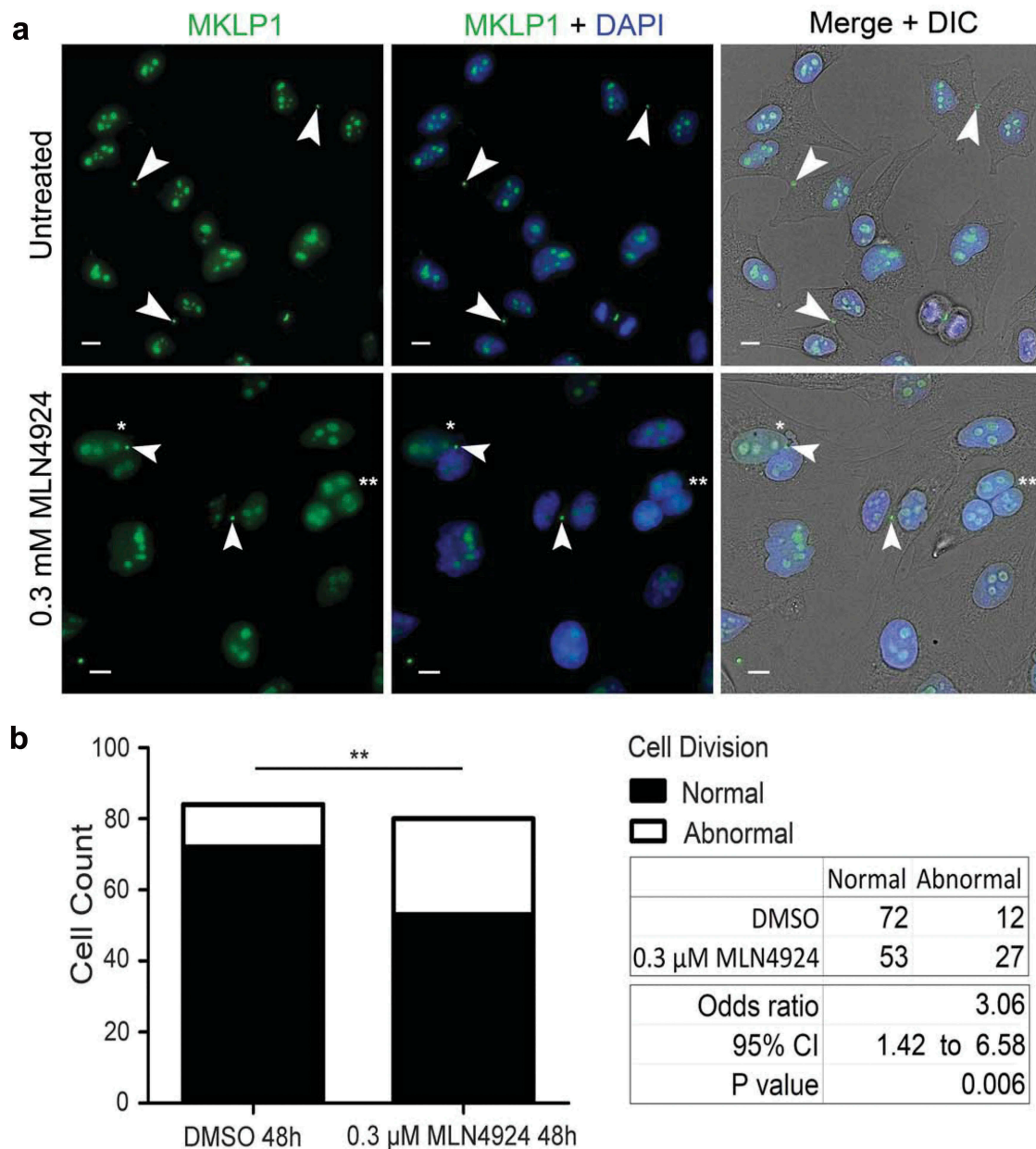


Figure 6. Chemical inhibition of neddylation in HeLa cells increases abnormal mitotic events. (a) Representative images of HeLa cells treated with vehicle (0.03% DMSO) or 0.3 μM MLN4924 for 48 h. MKLP1 localization at the midbody is indicated (red, white arrowheads), and DNA is indicated by DAPI staining (blue). Abnormal mitotic events, such as failed abscission resulting in binucleated (*) and multinucleated cells (**) are indicated with white asterisks. (b) The number of cells with Normal and Abnormal cell division was quantified and depicted as a stacked histogram; where abnormal cell division was defined as cells demonstrating asymmetric cell division (resulting in binucleated cells), lagging chromosomes and/or the presence of chromosomal bridges. Significance of the difference in the distributions between treated and untreated cells with respect to normal and abnormal cell division was determined by Fisher's exact test ** = $p < 0.01$.

increased nuclear size (Figure 1 and Supplemental Figure S2). In HeLa cells treated with MLN4924, we also characterized elevated protein levels of CDT1 and Geminin, G2 arrest and cells with >4N DNA content (Figures 1 and 2). These effects are attributed to reduced neddylation of the cullin-RING E3 ligases (CRL) resulting in reduced CRL

activity and the accumulation of CDT1 and other substrates, and indeed we observed both reduced bulk protein neddylation and reduced neddylation of cullin 1 (CUL1) (Figure S1). However, in previous studies in human cells the mitotic effects of MLN4924 were not characterized, nor has the COP9 signalosome (CSN) complex been localized

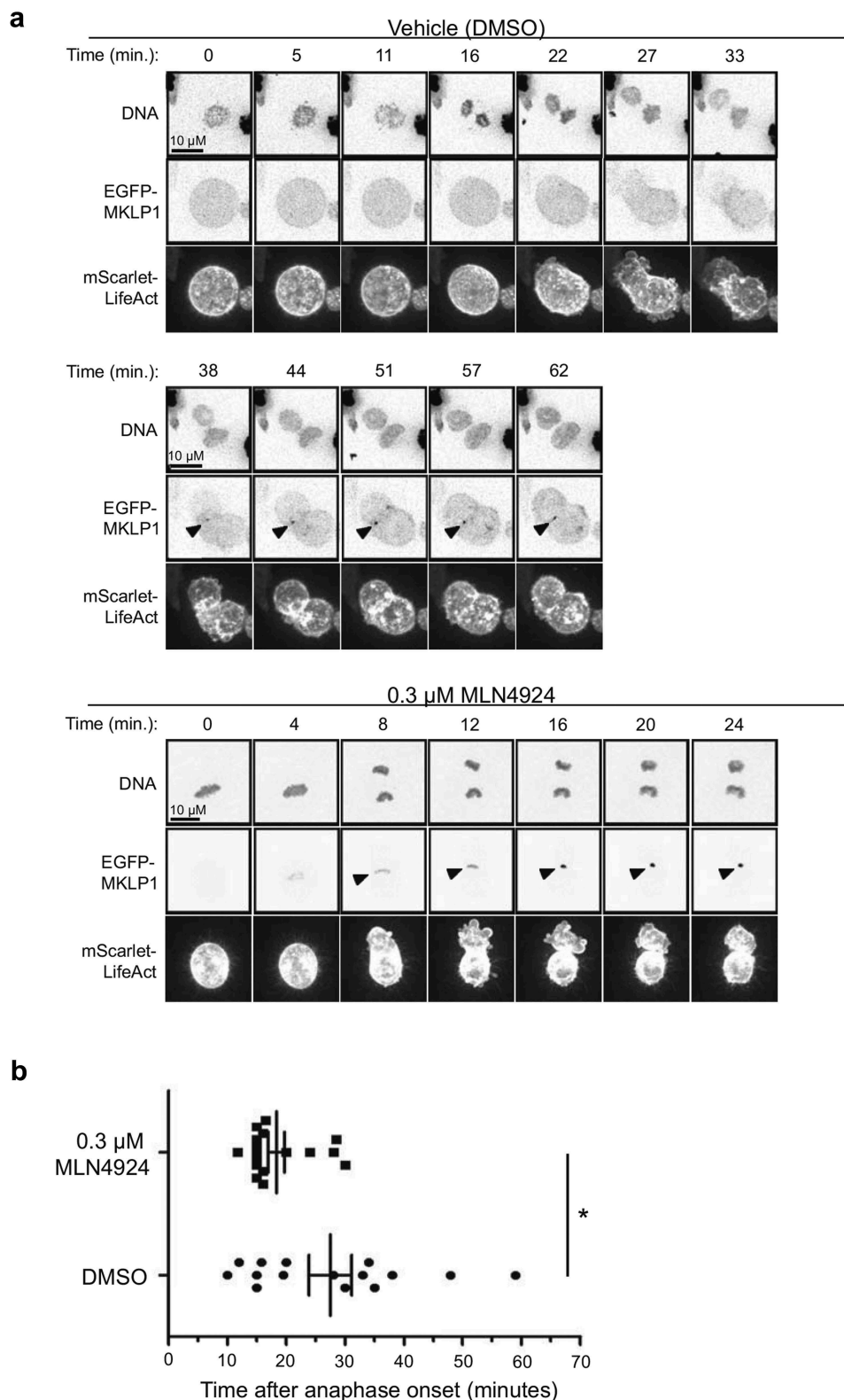


Figure 7. Chemical inhibition of neddylation in HeLa cells during mitosis leads to altered timing of the accumulation of MKLP1 at the cleavage furrow and midbody. (a) Mitotic HeLa cells expressing mScarlet-i-LifeAct were treated with vehicle (0.03% DMSO) or 0.3 μ M MLN4924 and followed over time by live-cell spinning disk confocal microscopy. DNA were stained with the viable dye SiR-DNA, and the actin cytoskeleton was visualized by mScarlet-i-LifeAct. MKLP1 accumulation at the midbody is indicated with a white arrowhead. (b) A horizontal scatter plot of the timing (in minutes) of MKLP1 accumulation to the cleavage furrow (and midbody) after the onset of anaphase is shown, where each dot represents one dividing cell, and the mean length of time and standard error are indicated. Significance was determined using an unpaired Student's t-test with Welch's correction. ** = $p < 0.01$.

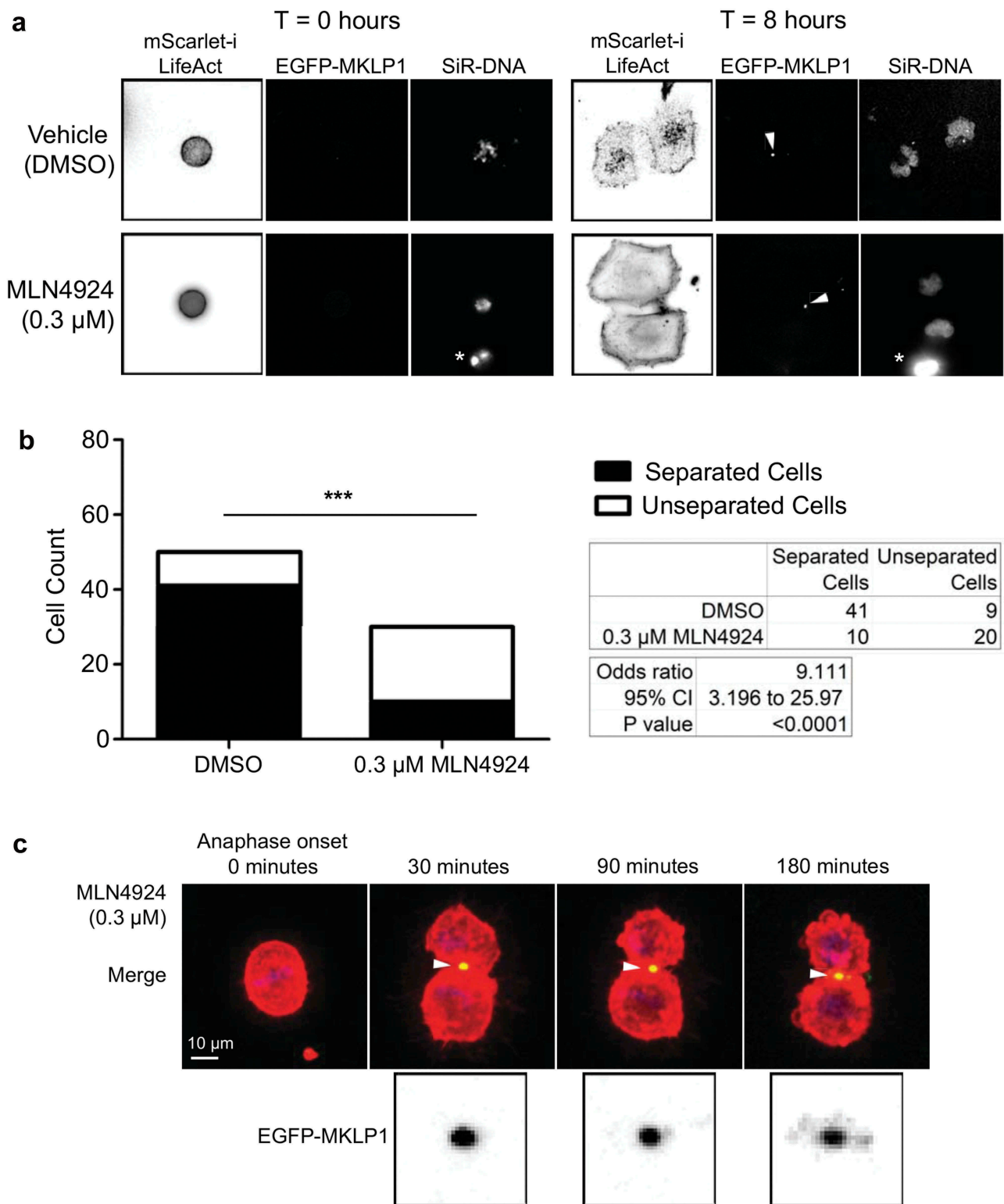


Figure 8. Chemical inhibition of neddylation of HeLa cells in mitosis results in delayed or failed abscission. (a) Representative images of HeLa cells expressing an actin cytoskeleton marker mScarlet-i-LifeAct and midbody marker EGFP-MKLP1 were stained with viable DNA dye SiR-DNA and treated with vehicle (0.03% DMSO) or 0.3 μ M MLN4924 at the onset of metaphase, and then followed for 8 h. (b) The number of cells completing cytokinesis (separated) versus the number of cells remaining joined by a cellular bridge with delayed or failed abscission marked by binucleated cells (unseparated) was quantified for HeLa cells treated with vehicle or MLN4924 in mitosis as in Panel A, and depicted as a stacked histogram. Significance between the number of delayed/failed abscission events occurring in the vehicle versus drug-treated cells was determined by Fisher's exact test. *** = $p < 0.0001$ (c) Representative images demonstrating how MKLP1 localization at the midbody becomes fragmented between anaphase and late telophase in a subset of MLN4924-treated cells, concomitant with abscission failure. White arrowheads indicate the position of MKLP1 at the midbody. An asterisk (*) indicates dead cells/debris.

at the midbody during cytokinesis. In the present study, we demonstrate for the first time that NEDD8 and CSN subunits colocalize with CUL1 and 3 at the cleavage furrow and midbody in HeLa (Figures 3–5) and RPE-1 cells (Supplemental Figures S3 and S4), and provide evidence supporting a role for ongoing neddylation during cytokinesis. Specifically, inhibition of neddylation by MLN4924 induces mitotic defects in asynchronously growing cells (Figure 6 and Supplemental Figure S5), and that treatment of metaphase cells with MLN4924 resulted in the early accumulation of MKLP1 at the midbody concomitant with abscission delay (or failure) and ultimately resulted in chromosome segregation defects including lagging chromosomes and binucleated cells (Figures 7–8). Thus, the increase in DNA content measured by flow cytometry seen with prolonged MLN4924 treatment in this and other studies (e.g. [48]) arises not only from endoreplication of DNA but also from mitotic defects elicited by inhibition of neddylation.

In addition to ongoing neddylation playing a role in mitosis and cytokinesis, the localization of the COP9 signalosome (CSN) at the midbody (Figures 4–6, Supplemental Figures S3 and S4) also implicates protein deneddylation at the cleavage furrow and midbody during cytokinesis. Previous studies have potentially implicated the CSN complex in mitosis through the localization of CSN subunits at centrosomes in human cells [49], which are known to play a role in mitotic spindle formation [50], and the mitotic spindle defects seen in *C. elegans* embryos during the first mitotic cell division after siRNA knock-down of CSN subunits [11]. However, our study is the first to demonstrate that the CSN can also localize to the midbody, and together with previous findings these data indicate that the COP9 signalosome may be considered an additional “chromosomal passenger” complex that localizes progressively from the centrosome to the cleavage furrow, presumably to regulate the activity of cullins as cells progress through mitosis and ultimately cytokinesis. In addition, given the mitotic defects induced by the inhibition of neddylation specifically in mitosis, and the detection of the CSN at the midbody, we speculate that cycle(s) of neddylation and deneddylation of the cullins or other protein

substrates may be critical to ensure the tight regulation of the protein stability of cullin substrates during cytokinesis.

The most likely cullins to be regulated by neddylation at the cleavage furrow and midbody are CUL1 and 3, both of which have been identified as components of the midbody [38–41]. The mitotic defects seen in our study after treatment of mitotic cells with MLN4924, including binucleated cells and failed cytokinesis, are also reminiscent of the effects of siRNA knock-down of CUL3 in human cells and in *C. elegans* [11,38], and siRNA knockdown of the neddylation complex component DCUN1D1/SCCRO [51]. AURKB, which regulates mitotic progression by phosphorylating a number of substrates involved in mitotic progression including MKLP1 [6], is also a substrate of CUL1 and CUL3 [38,39], and potentially could have altered stability with MLN4924 treatment. In asynchronous cells, AURKB levels do not appear to be affected by 4-h treatment with 1 μ M MLN4924, more than 3 times the dose used in this study [52]. However, a recent study by Huang et al., (2017) [51] indicates AURKB stability in mitosis can be affected by inhibition of neddylation. In this study knock-down of DCUN1D1/SCCRO, which promotes CUL3 activation and localization at the cleavage furrow, stabilized AURKB levels in mitotic cells, delaying the completion of cytokinesis [51]. Another candidate protein involved in cytokinesis that is also a substrate of CUL3 is KATNA1 (also known p60/Katanin in mammals and MEI-1 in *C. elegans*), which localizes to the mitotic spindle during mitosis and is responsible for severing microtubules [11,53]. KATNA1 localizes to the spindle midzone in anaphase and knock-down of CUL3 by siRNA results in accumulation of KATNA1, which is speculated to alter microtubule integrity and contribute mitotic defects [53].

In addition to regulation of cullin activity by neddylation during mitosis, we cannot discount direct neddylation of midbody components playing a role in their stability or localization. For example, MKLP1 ubiquitination, mediated by UBPY (known as USP8) (mono-ubiquitination) [54] and TRAF6 (possibly poly-ubiquitination) [42] could be altered directly by MKLP1 neddylation on acceptor lysines used for ubiquitination; a possibility supported by the recent evidence that MKLP1 may be neddylated at lysine 599 [55]. In an attempt to address this possibility, we immunoprecipitated GFP-tagged MKLP1 from

HeLa cells (Supplemental Figure S6). Whereas we could readily detect neddylated EGFP-CUL1 by immunoprecipitation from cells synchronized by double-thymidine block, we were unable to identify neddylated species of MKLP1. In any case, the early accumulation of MKLP1 that we observed at the mid-body when cells were treated with MLN4924 to inhibit *de novo* neddylation during mitosis is more consistent with the stabilization of MKLP1 in early anaphase, rather than increased degradation which one would expect if *de novo* neddylation of MKLP1 was countering its ubiquitination. Although beyond the scope of the present work, further study is warranted to confirm if MKLP1 is indeed modified at lysine 599 by ubiquitin or NEDD8, and what role this modification may play in mitosis.

Finally, given the important role of neddylation in regulating pathways in cancer development and progression, such as cell cycle regulation and DNA repair, neddylation and deneddylation mechanisms represent promising therapeutic targets for cancer treatment. For example, CSN subunits are overexpressed in multiple forms of cancer (CSN3 [56–60]:) (CSN5 [61]:) (CSN6 [62]:) and the inhibition of cullin-RING E3 ligases by MLN4924 is being employed in the treatment of multiple cancers [63,64]. However, the rationale for combination therapies that combine neddylation pathway inhibitors and conventional chemotherapy has been lacking. Our finding that MLN4924 can induce mitotic defects in cells suggests that inhibition of neddylation could synergize with specific chemotherapies that target proliferating cancer cells, such as the microtubule poisons vincristine and the taxanes [65]. In support of this concept, a recent clinical trial has demonstrated that MLN4924 has shown efficacy against advanced solid tumors when combined with the taxane paclitaxel and DNA damaging agent carboplatin [66]. Thus, our study provides a new rationale for combination therapies that employ anti-mitotic drugs with MLN4924.

Methods and materials

Reagents and antibodies

Transfection was performed using Lipofectamine 2000 (Invitrogen, 11668-019) following the

manufacturer's protocol by combining reagent (μL) with DNA (μg) at a 2:1 ratio. DMSO was purchased from Sigma-Aldrich (D2650). MLN4924 was purchased from Active Biochemicals (A-1139).

Antibodies rabbit anti-CUL1 (ab75812), rabbit anti-CUL3 (ab194584), rabbit anti-NEDD8 (ab81264), and rabbit anti-CSN4 (ab12322) were purchased from Abcam. Donkey anti-rabbit secondary antibodies conjugated to Alexa Fluor 488, 555, or 647 were purchased from Invitrogen (A-21206, A-31572 and A-31573, respectively).

Cell culture methods

The HeLa S3 and RPE-1 cell lines were obtained from ATCC (CCL-2.2 and CRL-4000, respectively) and cultured in Dulbecco's Modified Eagle Medium (DMEM) with 4.5 g/L D-glucose, L-Glutamine, and 100 mg/L sodium pyruvate (Gibco, 11995-065), and supplemented with 10% fetal bovine serum (Gibco, 12483-020) and 1% penicillin/streptomycin (Gibco, 15140-022). Tert-GM05757 cells were generated by Dellaire and colleagues and cultured as described previously [36].

DNA plasmids

ES-FUCCI was a gift from Pierre Neveu (Addgene plasmid #62451) [34]. pEGFP-C1-MKLP1 and pmCherry-C1-MKLP1 were gifts from Masanori Mishima (Addgene plasmid #70145 and #70154) [67,68]. pLifeAct_mScarlet-i_N1 was a gift from Dorus Gadella (Addgene plasmid #85056) [69]. CSN subunit cDNA was generated from total RNA by reverse transcription (Invitrogen One-step RT-PCR) using custom-designed primers (Supplementary Table S1) and cloned into pEGFP-C1 (Clontech); with the exception of COPS6, which was subcloned from pCOPS6-N-HA (B. Tse). CUL1-EGFP was generated by subcloning CUL1 from pcDNA3-myc3-CUL1 (a gift from Yue Xiong (Addgene plasmid #19896)) [70] in pEGFP-C1 as above.

Immunofluorescence microscopy

Cells cultured on No. 1.5 coverslips (Fisher Scientific 12–541-B) were rinsed with PBS and fixed with 4% paraformaldehyde (Electron Microscopy Services, 15710) for 20 min at room

temperature. Cells were then permeabilized with 0.05% Triton X-100 (Sigma-Aldrich, T9284) in PBS for 15 min. Blocking buffer consisted of 4% BSA in PBS. Vectashield (Vector Laboratories, H-1000) was used as the mounting medium. All imaging work was performed using a Marianas spinning-disk confocal microscope system (Intelligent Imaging Innovations) based on a Zeiss Axio Cell Observer equipped with a Yokagawa CSU-X1 spinning-disk unit and four laser lines (405, 488, 560 and 640 nm). Cells were observed using a 40X (1.3 NA) or 63X objective (1.4 NA) lens and images were recorded using an Evolve 512 electron-multiplying CCD (EMCCD) (Photometrics). Both image acquisition and processing were performed using Slidebook 6.0 (Intelligent Imaging Innovations).

Live cell imaging

Cells were cultured in CO₂-independent media (Gibco, 18045-088) supplemented with 1X GlutaMAXTM (Gibco, 35050-061), 10% FBS, and 1% Penicillin/Streptomycin. Cells were synchronized by double thymidine block using 2 mM thymidine (Sigma-Aldrich, T9250). Transfection was performed in between the first and second thymidine block. Cells were released from the second thymidine block and allowed to progress through the cell cycle until the population entered mitosis. Mitotic cells were harvested by mitotic shake-off [71] and resuspended in CO₂-independent media containing vehicle (DMSO) or 0.3 μM MLN4924 before transferring onto polyornithine (Sigma-Aldrich, P4957) labeled 35 mm glass bottom plates (FluoroDishTM, World Precision Instruments, FD35-100). Living cells were labeled with SiR-DNA (Cytoskeleton, CY-SC007) for 8 h to visualize DNA.

For Fluorescence Recovery after Photobleaching (FRAP) experiments, 100,000 cells were seeded on 35 mm glass bottom plates then transfected the next day. One day after transfection, cells maintained in CO₂-independent media (as above) were photobleached using a Vector Scan unit (Intelligent Imaging Innovations) equipped with a 488 nm laser, and images captured using a Marianas spinning-disk confocal microscope (Intelligent Imaging

Innovations) as described for immunofluorescence microscopy. Fluorescence recovery measurements were performed on Slidebook 6.0 (Intelligent Imaging Innovations) using their FRAP module.

Flow cytometry and cell cycle analysis

Trypsinized cells were pelleted by centrifugation at 1200 rpm (270 X g) for 6 min, washed in cold PBS and fixed in 70% ethanol at -20°C overnight. Before FACS analysis, cells were again pelleted and washed in PBS, and following centrifugation (as above) resuspended in PBS containing 50 μg/mL (75 μM) propidium iodide (Sigma-Aldrich, T1503) and 0.2 mg/mL RNaseA (Sigma-Aldrich, 6513) to a final cell concentration of 2 × 10⁶ cells/mL. The cells were incubated at 37°C for 20 min, then kept on ice prior to analysis using a FACSCalibur or FACSCanto II flow cytometer (BD Biosciences). Cell profiles were then determined from FACS data using Flowing Software Ver. 2.5.1 (Perttu Terho, Turku Centre for Biotechnology).

Western blotting

Whole cell lysates were prepared by direct lysis of cells in 1X RIPA buffer (150 mM NaCl, 1.0% IGEPAL[®] CA-630, 0.5% sodium deoxycholate, 0.1% SDS, 50 mM Tris, pH 8.0) (Sigma-Aldrich, R0278) supplemented with 1X Protease Inhibitor Cocktail (Sigma-Aldrich, P8340) and the phosphatase inhibitors sodium fluoride (10 mM) (Sigma-Aldrich, S1504) and sodium orthovanadate (1 mM) (Sigma-Aldrich, 450243). Lysates were then subjected to SDS-polyacrylamide gel electrophoresis (PAGE) and wet transfer (BioRad) to a nitrocellulose membrane (BioRad), prior to detection with primary and secondary antibodies diluted in 5% milk/PBS-Tween 20 (Sigma-Aldrich, P7949). Western blots were developed using an ECL detection kit (BioRad ClarityTM 1705061). Primary antibodies used were: mouse anti-β-actin (Sigma-Aldrich, A1978), rabbit anti-CUL1 (Abcam, ab75812), and rabbit anti-NEDD8 (Abcam, ab81264). Secondary antibodies purchased from Sigma-Aldrich were sheep anti-

mouse (A6782) and goat anti-rabbit (A6154) horse-radish peroxidase.

Cell viability assay

Two thousand cells were seeded into individual wells of a 96-well plate and allowed to adhere overnight. Treatment was applied to the wells for a total of 24 h. At hour 20, alamarBlue™ (Life Technologies, DAL1000) was applied to each well at 1/10 the total volume per well, and then returned to the 37°C incubator for 4 h. Emitted fluorescence was read at 590 nm using an Infinite M200 Pro plate reader (Tecan Group Ltd). To determine the relative change in fluorescence signal of each treatment in each biological replicate, the average background fluorescence was subtracted from the average fluorescence value, and then normalized to the vehicle control.

Data and statistical analysis

mCherry-CDT1 and Citrine-Geminin fluorescence intensity in Figure 1, nuclear area in Figure 2, and signal intensity across the midbody in Figures 3 and 4 were quantified using Fiji (ImageJ 1.52b) software [72]. Colour channels were separated for each image, and a threshold was applied on the DAPI channel to highlight nuclei. Sub-nuclear objects were excluded by applying a minimum size cut-off. The threshold was then applied to the other channels. Nucleus area and integrated density were measured for each object. The product of the nucleus area and background fluorescence (mean gray value) was then subtracted from the integrated density measurement to obtain the corrected value. Plot profiles across representative midbodies was performed by line-scan across the midbody (over y/x) for each channel, and intensity values were combined to generate line graphs. Fluorescently tagged proteins at the midbody in Figures 4 and 5 were quantified using SlideBook 6.0 software (Intelligent Imaging Innovations). All dot plots, bar or line graphs and statistics were generated using GraphPad Prism software Ver. 5 and/or Excel (Microsoft). A Fisher's exact test or a two-tailed Student's t-test (with or without Welch's correction for non-equal variance, as indicated) was used for significance testing between treatment groups.

Acknowledgments

G.D. is a senior Scientist of the Beatrice Hunter Cancer Research Institute (BHCRI). D.C. was supported by a Nova Scotia Graduate Scholarship. This work was funded by a Discovery grant awarded to G.D. from the Natural Sciences and Engineering Research Council of Canada (NSERC) (RGPIN 05616). All flow cytometry acquisition was performed at the Dalhousie Medical School's Core Flow Cytometry Facility.

Disclosure statement

No potential conflict of interest was reported by the authors.

Funding

This work was supported by the Natural Sciences and Engineering Research Council of Canada [RGPIN 05616].

ORCID

Graham Dellaire  <http://orcid.org/0000-0002-3466-6316>

References

- [1] Green RA, Paluch E, Oegema K. Cytokinesis in animal cells. *Annu Rev Cell Dev Biol.* 2012;28:29–58. PubMed PMID: 22804577.
- [2] Skop AR, Liu H, Yates J 3rd, et al. Dissection of the mammalian midbody proteome reveals conserved cytokinesis mechanisms. *Science.* 2004 Jul 2;305(5680):61–66. PubMed PMID: 15166316; PubMed Central PMCID: PMCPMC3679889.
- [3] Chen TC, Lee SA, Hong TM, et al. From midbody protein-protein interaction network construction to novel regulators in cytokinesis. *J Proteome Res.* 2009 Nov;8(11):4943–4953. PubMed PMID: 19799413.
- [4] Adams RR, Carmena M, Earnshaw WC. Chromosomal passengers and the (aurora) ABCs of mitosis. *Trends Cell Biol.* 2001 Feb;11(2):49–54. PubMed PMID: 11166196.
- [5] Zhu C, Bossy-Wetzel E, Jiang W. Recruitment of MKLP1 to the spindle midzone/midbody by INCENP is essential for midbody formation and completion of cytokinesis in human cells. *Biochem J.* 2005 Jul 15;389(Pt 2):373–381. PubMed PMID: 15796717; PubMed Central PMCID: PMCPMC1175114.
- [6] Guse A, Mishima M, Glotzer M. Phosphorylation of ZEN-4/MKLP1 by aurora B regulates completion of cytokinesis. *Curr Biol.* 2005 Apr 26;15(8):778–786. PubMed PMID: 15854913.
- [7] Fujiwara T, Bandi M, Nitta M, et al. Cytokinesis failure generating tetraploids promotes tumorigenesis in p53-null

- cells. *Nature*. 2005 Oct 13;437(7061):1043–1047. PubMed PMID: 16222300.
- [8] Nigg EA. Mitotic kinases as regulators of cell division and its checkpoints. *Nat Rev Mol Cell Biol*. 2001 Jan;2(1):21–32. . PubMed PMID: 11413462.
- [9] Hochstrasser M. Origin and function of ubiquitin-like proteins. *Nature*. 2009 Mar 26;458(7237):422–429. . PubMed PMID: 19325621; PubMed Central PMCID: PMC2819001.
- [10] Zhang XD, Goeres J, Zhang H, et al. SUMO-2/3 modification and binding regulate the association of CENP-E with kinetochores and progression through mitosis. *Mol Cell*. 2008 Mar 28;29(6):729–741. PubMed PMID: 18374647; PubMed Central PMCID: PMC2366111.
- [11] Pintard L, Kurz T, Glaser S, et al. Neddylation and deneddylation of CUL-3 is required to target MEI-1/Katanin for degradation at the meiosis-to-mitosis transition in *C. elegans*. *Curr Biol*. 2003 May 27;13(11):911–921. PubMed PMID: 12781129.
- [12] Lydeard JR, Schulman BA, Harper JW. Building and remodelling Cullin-RING E3 ubiquitin ligases. *EMBO Rep*. 2013 Dec;14(12):1050–1061. . PubMed PMID: 24232186; PubMed Central PMCID: PMC3849489.
- [13] Balachandran RS, Heighington CS, Starostina NG, et al. The ubiquitin ligase CRL2ZYG11 targets cyclin B1 for degradation in a conserved pathway that facilitates mitotic slippage. *J Cell Biol*. 2016 Oct 24;215(2):151–166. PubMed PMID: 27810909; PubMed Central PMCID: PMC4508464.
- [14] Rizzardi LF, Cook JG. Flipping the switch from G1 to S phase with E3 ubiquitin ligases. *Genes Cancer*. 2012 Nov;3(11–12):634–648. PubMed PMID: 23634252; PubMed Central PMCID: PMC3636747.
- [15] Nishitani H, Sugimoto N, Roukos V, et al. Two E3 ubiquitin ligases, SCF-Skp2 and DDB1-Cul4, target human Cdt1 for proteolysis. *Embo J*. 2006 Mar 8;25(5):1126–1136. PubMed PMID: 16482215; PubMed Central PMCID: PMC1409712.
- [16] Li X, Zhao Q, Liao R, et al. The SCF(Skp2) ubiquitin ligase complex interacts with the human replication licensing factor Cdt1 and regulates Cdt1 degradation. *J Biol Chem*. 2003 Aug 15;278(33):30854–30858. PubMed PMID: 12840033.
- [17] McGarry TJ, Kirschner MW. Geminin, an inhibitor of DNA replication, is degraded during mitosis. *Cell*. 1998 Jun 12;93(6):1043–1053. PubMed PMID: 9635433.
- [18] Chung D, Dellaire G. The role of the COP9 signalosome and neddylation in DNA damage signaling and repair. *Biomolecules*. 2015 Sep 30;5(4):2388–2416. PubMed PMID: 26437438; PubMed Central PMCID: PMC4693240.
- [19] Enchev RI, Schulman BA, Peter M. Protein neddylation: beyond cullin-RING ligases. *Nat Rev Mol Cell Biol*. 2015 Jan;16(1):30–44. PubMed PMID: 25531226; PubMed Central PMCID: PMC25131867.
- [20] Cope GA, Deshaies RJ. COP9 signalosome: a multifunctional regulator of SCF and other cullin-based ubiquitin ligases. *Cell*. 2003 Sep 19;114(6):663–671. PubMed PMID: 14505567.
- [21] Schwechheimer C. The COP9 signalosome (CSN): an evolutionary conserved proteolysis regulator in eukaryotic development. *Biochim Biophys Acta*. 2004 Nov 29;1695(1–3):45–54. . PubMed PMID: 15571808.
- [22] Wei N, Tsuge T, Serino G, et al. The COP9 complex is conserved between plants and mammals and is related to the 26S proteasome regulatory complex. *Curr Biol*. 1998 Jul 30;8(16):919–922. Aug 13;(). PubMed PMID: 9707402. .
- [23] Wu K, Yamoah K, Dolios G, et al. DEN1 is a dual function protease capable of processing the C terminus of Nedd8 and deconjugating hyper-neddylated CUL1. *J Biol Chem*. 2003 Aug 1;278(31):28882–28891. PubMed PMID: 12759363.
- [24] Mendoza HM, Shen LN, Botting C, et al. NEDP1, a highly conserved cysteine protease that deNEDDylates Cullins. *J Biol Chem*. 2003 Jul 11;278(28):25637–25643. PubMed PMID: 12730221.
- [25] Lingaraju GM, Bunker RD, Cavadini S, et al. Crystal structure of the human COP9 signalosome. *Nature*. 2014 Aug 14;512(7513):161–165. PubMed PMID: 25043011.
- [26] Kotiguda GG, Weinberg D, Dessau M, et al. The organization of a CSN5-containing subcomplex of the COP9 signalosome. *J Biol Chem*. 2012 Dec 7;287(50):42031–42041. PubMed PMID: 23086934; PubMed Central PMCID: PMC3516749.
- [27] Pan L, Wang S, Lu T, et al. Protein competition switches the function of COP9 from self-renewal to differentiation. *Nature*. 2014 Oct 9;514(7521):233–236. PubMed PMID: 25119050.
- [28] Wei N, Serino G, Deng XW. The COP9 signalosome: more than a protease. *Trends Biochem Sci*. 2008 Dec;33(12):592–600. PubMed PMID: 18926707.
- [29] Soucy TA, Smith PG, Milhollen MA, et al. An inhibitor of NEDD8-activating enzyme as a new approach to treat cancer. *Nature*. 2009 Apr 9;458(7239):732–736. PubMed PMID: 19360080.
- [30] Lin JJ, Milhollen MA, Smith PG, et al. NEDD8-targeting drug MLN4924 elicits DNA rereplication by stabilizing Cdt1 in S phase, triggering checkpoint activation, apoptosis, and senescence in cancer cells. *Cancer Res*. 2010 Dec 15;70(24):10310–10320. PubMed PMID: 21159650; PubMed Central PMCID: PMC3059213.
- [31] Han K, Wang Q, Cao H, et al. The NEDD8-activating enzyme inhibitor MLN4924 induces G2 arrest and apoptosis in T-cell acute lymphoblastic leukemia. *Oncotarget*. 2016 Apr 26;7(17):23812–23824. PubMed PMID: 26993774; PubMed Central PMCID: PMC45029665.
- [32] Yang D, Tan M, Wang G, et al. The p21-dependent radiosensitization of human breast cancer cells by MLN4924, an investigational inhibitor of NEDD8 activating enzyme. *PLoS One*. 2012;7(3):e34079. PubMed PMID: 22457814; PubMed Central PMCID: PMC3310880.
- [33] Sakaue-Sawano A, Kurokawa H, Morimura T, et al. Visualizing spatiotemporal dynamics of multicellular

- cell-cycle progression. *Cell*. 2008 Feb 8;132(3):487–498. PubMed PMID: 18267078.
- [34] Sladitschek HL, Neveu PA. MXS-chaining: a highly efficient cloning platform for imaging and flow cytometry approaches in mammalian systems. *PLoS One*. 2015;104:e0124958. PubMed PMID: 25909630; PubMed Central PMCID: PMCPCMC4409215
- [35] Rulina AV, Mittler F, Obeid P, et al. Distinct outcomes of CRL-Nedd8 pathway inhibition reveal cancer cell plasticity. *Cell Death Dis*. 2016 Dec 1;7(12):e2505. PubMed PMID: 27906189; PubMed Central PMCID: PMCPCMC5261022.
- [36] Dellaire G, Ching RW, Ahmed K, et al. Promyelocytic leukemia nuclear bodies behave as DNA damage sensors whose response to DNA double-strand breaks is regulated by NBS1 and the kinases ATM, Chk2, and ATR. *J Cell Biol*. 2006 Oct 9;175(1):55–66. PubMed PMID: 17030982; PubMed Central PMCID: PMCPCMC2064496.
- [37] Conery AR, Harlow E. High-throughput screens in diploid cells identify factors that contribute to the acquisition of chromosomal instability. *Proc Natl Acad Sci USA*. 2010 Aug 31;107(35):15455–15460. PubMed PMID: 20713694; PubMed Central PMCID: PMCPCMC2932617.
- [38] Sumara I, Quadroni M, Frei C, et al. A Cul3-based E3 ligase removes Aurora B from mitotic chromosomes, regulating mitotic progression and completion of cytokinesis in human cells. *Dev Cell*. 2007 Jun;12(6):887–900. PubMed PMID: 17543862.
- [39] Maerki S, Olma MH, Staubli T, et al. The Cul3-KLHL21 E3 ubiquitin ligase targets aurora B to midzone microtubules in anaphase and is required for cytokinesis. *J Cell Biol*. 2009 Dec 14;187(6):791–800. PubMed PMID: 19995937; PubMed Central PMCID: PMCPCMC2806313.
- [40] Freed E, Lacey KR, Huie P, et al. Components of an SCF ubiquitin ligase localize to the centrosome and regulate the centrosome duplication cycle. *Genes Dev*. 1999 Sep 1;13(17):2242–2257. PubMed PMID: 10485847; PubMed Central PMCID: PMCPCMC316987.
- [41] Chen BB, Glasser JR, Coon TA, et al. Skp-cullin-F box E3 ligase component FBXL2 ubiquitinates Aurora B to inhibit tumorigenesis. *Cell Death Dis*. 2013 Aug 8;4:e759. PubMed PMID: 23928698; PubMed Central PMCID: PMCPCMC3763433.
- [42] Isakson P, Lystad AH, Breen K, et al. TRAF6 mediates ubiquitination of KIF23/MKLP1 and is required for midbody ring degradation by selective autophagy. *Autophagy*. 2013 Dec;9(12):1955–1964. PubMed PMID: 24128730.
- [43] Tong S, Si Y, Yu H, et al. MLN4924 (Pevonedistat), a protein neddylation inhibitor, suppresses proliferation and migration of human clear cell renal cell carcinoma. *Sci Rep*. 2017 Jul 17;7(1):5599. 10.1038/s41598-017-06098-y. PubMed PMID: 28717191; PubMed Central PMCID: PMCPCMC5514088.
- [44] Luo Z, Yu G, Lee HW, et al. The Nedd8-activating enzyme inhibitor MLN4924 induces autophagy and apoptosis to suppress liver cancer cell growth. *Cancer Res*. 2012 Jul 1;72(13):3360–3371. PubMed PMID: 22562464.
- [45] Zhang Y, Shi CC, Zhang HP, et al. MLN4924 suppresses neddylation and induces cell cycle arrest, senescence, and apoptosis in human osteosarcoma. *Oncotarget*. 2016 Jul 19;7(29):45263–45274. PubMed PMID: 27223074; PubMed Central PMCID: PMCPCMC5216721.
- [46] Ma T, Chen Y, Zhang F, et al. RNF111-dependent neddylation activates DNA damage-induced ubiquitination. *Mol Cell*. 2013 Mar 7;49(5):897–907. PubMed PMID: 23394999; PubMed Central PMCID: PMCPCMC3595365.
- [47] Brown JS, Lukashchuk N, Sczaniecka-Clift M, et al. Neddylation promotes ubiquitylation and release of Ku from DNA-damage sites. *Cell Rep*. 2015 May 5;11(5):704–714. PubMed PMID: 25921528; PubMed Central PMCID: PMCPCMC4431666.
- [48] Milhollen MA, Narayanan U, Soucy TA, et al. Inhibition of NEDD8-activating enzyme induces rereplication and apoptosis in human tumor cells consistent with deregulating CDT1 turnover. *Cancer Res*. 2011 Apr 15;71(8):3042–3051. PubMed PMID: 21487042.
- [49] Peth A, Boettcher JP, Dubiel W. Ubiquitin-dependent proteolysis of the microtubule end-binding protein 1, EB1, is controlled by the COP9 signalosome: possible consequences for microtubule filament stability. *J Mol Biol*. 2007 Apr 27;368(2):550–563. PubMed PMID: 17350042.
- [50] Wang G, Jiang Q, Zhang C. The role of mitotic kinases in coupling the centrosome cycle with the assembly of the mitotic spindle. *J Cell Sci*. 2014 Oct 1;127(Pt 19):4111–4122. PubMed PMID: 25128564.
- [51] Huang G, Kaufman AJ, Xu K, et al. Squamous cell carcinoma-related oncogene (SCCRO) neddylates Cul3 protein to selectively promote midbody localization and activity of Cul3(KLHL21) protein complex during abscission. *J Biol Chem*. 2017 Sep 15;292(37):15254–15265. PubMed PMID: 28620047; PubMed Central PMCID: PMCPCMC5602386.
- [52] Huang HT, Dobrovolsky D, Paulk J, et al. A chemoproteomic approach to query the degradable kinome using a multi-kinase degrader. *Cell Chem Biol*. 2018 Jan 18;25(1):88–99 e6. PubMed PMID: 29129717.
- [53] Cummings CM, Bentley CA, Perdue SA, et al. The Cul3/Klhdc5 E3 ligase regulates p60/katanin and is required for normal mitosis in mammalian cells. *J Biol Chem*. 2009 Apr 24;284(17):11663–11675. PubMed PMID: 19261606; PubMed Central PMCID: PMCPCMC2670170.
- [54] Pohl C, Jentsch S. Final stages of cytokinesis and midbody ring formation are controlled by BRUCE. *Cell*. 2008 Mar 7;132(5):832–845. PubMed PMID: 18329369.
- [55] Coleman KE, Bekes M, Chapman JR, et al. SENP8 limits aberrant neddylation of NEDD8 pathway components to

- promote cullin-RING ubiquitin ligase function. *Elife*. 2017 May 5;6. PubMed PMID: 28475037; PubMed Central PMCID: PMC5419743.
- [56] Hong Y, Huang X, An L, et al. Overexpression of COPS3 promotes clear cell renal cell carcinoma progression via regulation of phospho-AKT(Thr308), cyclin D1 and Caspase-3. *Exp Cell Res*. 2018 Feb 23. PubMed PMID: 29477618. DOI:10.1016/j.yexcr.2018.02.025
- [57] Yan T, Tang G, Ren T, et al. RNAi-mediated COPS3 gene silencing inhibits metastasis of osteogenic sarcoma cells. *Cancer Gene Ther*. 2011 Jun;18(6):450–456. PubMed PMID: 21436869; PubMed Central PMCID: PMC3097431.
- [58] Yu YS, Tang ZH, Pan QC, et al. Inhibition of Csn3 expression induces growth arrest and apoptosis of hepatocellular carcinoma cells. *Cancer Chemother Pharmacol*. 2012 May;69(5):1173–1180. PubMed PMID: 22237956.
- [59] van Dartel M, Redeker S, Bras J, et al. Overexpression through amplification of genes in chromosome region 17p11.2 approximately p12 in high-grade osteosarcoma. *Cancer Genet Cytogenet*. 2004 Jul 1;152(1):8–14. PubMed PMID: 15193436.
- [60] Pang J, Yan X, Cao H, et al. Knockdown of COPS3 inhibits lung cancer tumor growth in nude mice by blocking cell cycle progression. *J Cancer*. 2017;8(7):1129–1136. PubMed PMID: 28607586; PubMed Central PMCID: PMC5463426.
- [61] Zhang H, Zhong A, Sun J, et al. COPS5 inhibition arrests the proliferation and growth of serous ovarian cancer cells via the elevation of p27 level. *Biochem Biophys Res Commun*. 2017 Nov 4;493(1):85–93. PubMed PMID: 28919423.
- [62] Zhao R, Yeung SC, Chen J, et al. Subunit 6 of the COP9 signalosome promotes tumorigenesis in mice through stabilization of MDM2 and is upregulated in human cancers. *J Clin Invest*. 2011 Mar;121(3):851–865. PubMed PMID: 21317535; PubMed Central PMCID: PMC3049400.
- [63] Soucy TA, Smith PG, Rolfe M. Targeting NEDD8-activated cullin-RING ligases for the treatment of cancer. *Clin Cancer Res*. 2009 Jun 15;15(12):3912–3916. 10.1158/1078-0432.CCR-09-0343. PubMed PMID: 19509147.
- [64] Zhou L, Zhang W, Sun Y, et al. Protein neddylation and its alterations in human cancers for targeted therapy. *Cell Signal*. 2018 Apr;44:92–102. PubMed PMID: 29331584; PubMed Central PMCID: PMC5829022.
- [65] Rao CV, Kurkjian CD, Yamada HY. Mitosis-targeting natural products for cancer prevention and therapy. *Curr Drug Targets*. 2012 Dec;13(14):1820–1830. PubMed PMID: 23140292.
- [66] Lockhart AC, Bauer TM, Aggarwal C, et al. Phase Ib study of pevonedistat, a NEDD8-activating enzyme inhibitor, in combination with docetaxel, carboplatin and paclitaxel, or gemcitabine, in patients with advanced solid tumors. *Invest New Drugs*. 2018 May 21;37(1):87–97. PubMed PMID: 29781056.
- [67] Douglas ME, Davies T, Joseph N, et al. Aurora B and 14-3-3 coordinately regulate clustering of centralspindlin during cytokinesis. *Curr Biol*. 2010 May 25;20(10):927–933. PubMed PMID: 20451386; PubMed Central PMCID: PMC3348768.
- [68] Joseph N, Hutterer A, Poser I, et al. ARF6 GTPase protects the post-mitotic midbody from 14-3-3-mediated disintegration. *Embo J*. 2012 May 30;31(11):2604–2614. PubMed PMID: 22580824; PubMed Central PMCID: PMC3365424.
- [69] Bindels DS, Haarbosch L, van Weeren L, et al. mScarlet: a bright monomeric red fluorescent protein for cellular imaging. *Nat Methods*. 2017 Jan;14(1):53–56. PubMed PMID: 27869816.
- [70] Ohta T, Michel JJ, Schottelius AJ, et al. ROC1, a homolog of APC11, represents a family of cullin partners with an associated ubiquitin ligase activity. *Mol Cell*. 1999 Apr;3(4):535–541. PubMed PMID: 10230407.
- [71] Terasima T, Tolmach LJ. Growth and nucleic acid synthesis in synchronously dividing populations of HeLa cells. *Exp Cell Res*. 1963 Apr;30:344–362. PubMed PMID: 13980637
- [72] Schindelin J, Arganda-Carreras I, Frise E, et al. Fiji: an open-source platform for biological-image analysis. *Nat Methods*. 2012 Jun 28;9(7):676–682. PubMed PMID: 22743772; PubMed Central PMCID: PMC3855844.